Mechanical Systems and Signal Processing 25 (2011) 360–372

Contents lists available at ScienceDirect

Mechanical Systems and Signal Processing

journal homepage: www.elsevier.com/locate/jnlabr/ymssp

Electrical motor current signal analysis using a modified bispectrum for fault diagnosis of downstream mechanical equipment

F. Gu [a,*], Y. Shao [b], N. Hu [c], A. Naid [a], A.D. Ball [a]

[a] Centre for Diagnostic Engineering, University of Huddersfield, UK
[b] The State Key Lab of Mechanical Transmission, Chonqing University, Chongqing, PR China
[c] School of Mechatronics Engineering and Automation, National University of Defense Technology, Changsha, Hunan, PR China

ARTICLE INFO

Article history:
Received 7 December 2009
Received in revised form
6 July 2010
Accepted 10 July 2010
Available online 16 July 2010

Keywords:
Reciprocating compressor
Modified bispectrum
Kurtosis
Motor current signature analysis

ABSTRACT

This paper presents the use of the induction motor current to identify and quantify common faults within a two-stage reciprocating compressor based on bispectrum analysis. The theoretical basis is developed to understand the nonlinear characteristics of current signals when the motor undertakes a varying load under different faulty conditions. Although conventional bispectrum representation of current signal allows the inclusion of phase information and the elimination of Gaussian noise, it produces unstable results due to random phase variation of the sideband components in the current signal. A modified bispectrum based on the amplitude modulation feature of the current signal is then adopted to combine both lower sidebands and higher sidebands simultaneously and hence characterise the current signal more accurately. Based on this new bispectrum analysis a more effective diagnostic feature, namely normalised bispectral peak, is developed for fault classification. In association with the kurtosis value of the raw current signal, the bispectrum feature gives rise to reliable fault classification results. In particular, the low feature values can differentiate the belt looseness from the other fault cases and different degrees of discharge valve leakage and inter-cooler leakage can be separated easily using two linear classifiers. This work provides a novel approach to the analysis of stator current for the diagnosis of motor drive faults from downstream driving equipment.

Crown Copyright © 2010 Published by Elsevier Ltd. All rights reserved.

1. Introduction

Induction machine stator current signals have been used widely to determine the health of the induction machine since the early 1980s [1]. A limited amount of work has been undertaken in using the current signals to investigate the potential of using the induction machine as a means of assessing the condition of downstream driven equipment. In [2], it was shown that the influence of mechanical problems that result in rotor disturbances can be detected through the changes in the induction machine stator current. Further in [3], it was shown that the induction machine stator current can be used to detect the presence of load imbalance as well. In [4], a large-scale test involving the on-line monitoring of 120 induction machines in a coal preparation plant using supply parameters was presented. The outcomes were sufficiently promising to suggest that there are serious opportunities for the techniques to be exploited, especially using the effective negative sequence impedance. Further, it has been shown that the induction machine supply current can contain components

* Corresponding author. Tel.: +44 1474 473548; fax: +44 1484 473075.
E-mail addresses: f.gu@hud.ac.uk, fengshou_gu@hotmail.com (F. Gu).

0888-3270/$ - see front matter Crown Copyright © 2010 Published by Elsevier Ltd. All rights reserved.
doi:10.1016/j.ymssp.2010.07.004

related to abnormalities in equipment such as compressors, pumps, rolling mills, mixers, crushers, fans, blowers and material conveyors[5] and the technique has been used to detect specific axial flow compressor problems [6]. It has also been found that rotational frequency components of the driving induction machine are present in the supply current spectra [12,20] and can be used to detect damages from mechanical components such as bearings and gears.

In all these publications, the use of the motor supply parameters for the detection of faults in an equipment train has been limited in that no deterministic approaches have been demonstrated. One of the main reasons for this lack of diagnostic clarity is that the harmonic content and noise contained within an induction machine supply parameter, and in particular the stator current, is high and that traditional two-dimensional spectral analysis techniques can be insufficient to properly correlate the stator current data with faulty conditions. Therefore, many researchers have investigated other alternatives for analysing current signals for more reliable diagnosis. The discrete wavelet transform (DWT) has been applied to the current during a load reduction transient process [20] and shown that DWT is effective in detecting the local gear fault of differing severity. In addition, the DWT has also been used to analyse the current signals from start-up transients [21,22] and demonstrated an impressive performance in detecting different motors fault. The empirical mode decomposition (EMD) has also been evaluated to be capable of detecting faults from motors[23]. These achievements have shown that it is promising to obtain more accurate diagnosis by using methods other than the traditional spectral analysis.

Higher order spectra (HOS) are useful signal processing tools that have shown [7,8] significant benefits over traditional spectral analyses because HOS have nonlinear system identification, phase information retention and Gaussian noise elimination properties. The application of HOS techniques in condition monitoring has been reported in [9,10] and it is clear that multi-dimensional HOS measures can contain more useful information than traditional two-dimensional spectral measures for diagnostic purposes. Further, in [10], it was shown that these measures could be used in a deterministic manner to predict the HOS components of induction machine vibration sensitive to a number of fault conditions. Additionally, it was demonstrated that the HOS measures were more sensitive to the fault conditions than traditional spectral analysis. However, these techniques have not been extended to include induction machine supply parameter investigations or faults on the downstream driven equipment train. Especially, the theoretical basis of using HOS for analysing supply parameters has not been addressed in previous work.

This paper provides the details of applying HOS to current signals for the detection and diagnosis of the faults from downstream driven equipment. A theoretical basis is developed to predict the frequency components of the motor phase current under both health and seeded faults. Experimental investigations are based on a reciprocating compressor and four common fault conditions are investigated over a wide range of discharge pressure conditions. The bispectrum signal processing tools are then developed to characterise the currents signals for identifying both the presence and magnitude of the seeded faults.

2. Electrical motor current signal

To study possible nonlinear effect in current signals for applying HOS, the electromagnetic relationships are examined in only phase A, one of the three phases of a power supply system, with neglecting the higher order harmonics. By referring to supply voltage signal, the current signal in phase A for a health motor drive can be expressed [17,18] as

$$i_A = \sqrt{2} I \cos(2\pi f_s t - \alpha_I) \tag{1}$$

Correspondingly, the magnetic flux in motor stator is

$$\phi_A = \sqrt{2} \phi \cos(2\pi f_s t - \alpha_\phi) \tag{2}$$

The electrical torque produced by the interaction between the current and flux can be expressed as

$$T = 3P\phi I \sin(\alpha_I - \alpha_\phi) \tag{3}$$

where I and ϕ denote the root mean squared (RMS) amplitudes of the supply current and linkage flux, respectively, α_I and α_ϕ are the phases of the current and flux referring to supply voltage, f_s is the fundamental frequency of electrical supply and P is the number of pole pairs. If there is a fault occurring in the rotor system including motor rotor and rotational components connected to the rotor mechanically, there will be an additional torque component oscillating around the electric torque. Supposing that the additional torque ΔT is a sinusoidal wave with a frequency f_F, current amplitude I_F and phase α_F, the oscillatory torque can be obtained using Eq. (3):

$$\Delta T = 3P\phi I_F \sin[2\pi f_F t - (\alpha_I - \alpha_\phi) - \alpha_F] \tag{4}$$

Correspondingly, this oscillatory torque causes speed fluctuation. From the motor torque balance equation, the speed fluctuation due to this oscillatory torque can be derived as

$$\Delta\omega = \frac{P}{J}\int \Delta T\, dt = -\frac{3P^2\phi I_F}{2\pi f_F J}\cos\left[2\pi f_F t - (\alpha_I - \alpha_\phi) - \alpha_F\right] \tag{5}$$

and the angular oscillation is

$$\Delta\alpha_F = \int \Delta\omega\, dt = \frac{3P^2\phi I_F}{4\pi^2 f_F^2 J}\sin\left[2\pi f_F t - (\alpha_I - \alpha_\phi) - \alpha_F\right] \tag{6}$$

where J is the inertia of the rotor system. This angular variation produces phase modulation to the linkage flux and Eq. (2) becomes

$$\phi_A^F = \sqrt{2}\phi\cos\{2\pi f_s t-\alpha_\phi-\Delta\phi\sin[2\pi f_F t-(\alpha_I-\alpha_\phi)-\alpha_F]\} \tag{7}$$

where $\Delta\phi = 3P^2\phi I_F/4\pi^2 f_F^2 J$. This shows that the flux wave contains nonlinear effects because of the fault in the rotor system. This nonlinear interaction of linkage flux will produce corresponding electromagnetic force (EMF) and hence induce a nonlinear current signal in the stator.

Considering $\Delta\alpha_F$ is very small, resulting in $\cos(\Delta\alpha_F)\approx 1$ and $\sin(\Delta\alpha_F)\approx\Delta\alpha_F$, the linkage flux now can be simplified and examined in three components explicitly:

$$\begin{aligned}\phi_A^F &\approx \sqrt{2}\phi\cos(2\pi f_s t-\alpha_\phi)+\sqrt{2}\phi\,\Delta\alpha_F\sin(2\pi f_s t-\alpha_\phi)\\ &= \sqrt{2}\phi\cos(2\pi f_s t-\alpha_\phi)\\ &+\sqrt{2}\phi\,\Delta\phi\cos[2\pi(f_s-f_F)t-\alpha_I-\alpha_F]\\ &-\sqrt{2}\phi\,\Delta\phi\cos[2\pi(f_s+f_F)t-2\alpha_\phi+\alpha_I-\alpha_F]\end{aligned} \tag{8}$$

Eq. (8) shows that the flux contains not only the fundamental part but also sidebands around the fundamental frequency. This simplified flux allows the current expression to be obtained based on the motor equivalent circuit [17]:

$$\begin{aligned}i_A^F &= \sqrt{2}I\cos(2\pi f_s t-\alpha_I)\\ &+\sqrt{2}I_l\cos[2\pi(f_s-f_F)t-\alpha_I-\alpha_F-\varphi]\\ &-\sqrt{2}I_r\cos[2\pi(f_s+f_F)t-2\alpha_\phi+\alpha_I-\alpha_F-\varphi]\end{aligned} \tag{9}$$

where φ is the angular displacement of motor equivalent circuit impedance at supply frequency, I_l and I_r are the RMS values of the lower sideband component and the upper sideband component, respectively, which are the currents induced by the back-EMF voltages produced by the flux variations at frequencies of f_s-f_F and f_s+f_F This simplified expression of current signal is employed widely for motor fault condition monitoring. By checking the amplitude of the sideband through spectrum calculation, various faults such as rotor bar breakage and eccentricity can be diagnosed with a high degree of accuracy. However, conventional spectrum uses amplitude information only and overlooks the phase effect which also contains fault information, as shown in Eq. (9). The consequence of ignoring phase information may degrade diagnosis performance for the case of incipient faults when the sideband amplitude is very small and masked by various random noises. This is particularly true for diagnosing faults from downstream mechanical system. Fortunately, bispectrum analysis allows the retention of both the amplitude and the phase information, the suppression of random noise and the identification of nonlinear effects. This study thus focuses on using bispectrum to analyse the current signals from a reciprocating compressor in diagnosing several common faults.

A reciprocating compressor system consists of typically an induction motor, a belt transmitter and a multi-cylinder compressor. The compressor has two basic working processes: compression and expansion. Previous studies [11,13] show that the working process gives rise to a periodically varying load to the driving motor due to the compressor requiring more power in compression than in the expansion. This varying load results in high oscillation in the measured current signal. Following Eq. (9), the current signal measured can be expressed by denoting the various angular displacements with α_l and α_r the lower and higher sideband components, respectively:

$$i_A = \sqrt{2}I\cos 2\pi f_s t+\sqrt{2}I_l\cos[2\pi(f_s-f_F)t-\alpha_l]+\sqrt{2}I_r\cos[2\pi(f_s+f_F)t-\alpha_r] \tag{10}$$

In Eq. (10) two frequency components: f_s-f_F and f_s+f_F are distributed symmetrically around the supply frequency, showing that the phase current signal from the compressor is similar to the form of an amplitude modulation (AM). However, because $\alpha_l\neq\alpha_r$ and $I_l\neq I_r$, Eq. (10) is not a pure AM process because of the phase angle difference between the sideband pair. As shown in [17,18], the upper sideband component results from the lower sideband component due to a nonlinear effect caused by the interaction of magnetic flux, load and speed fluctuations. Their angular displacements are linked but have an angular difference, which is governed by both the phase of magnetic flux and the phase of the equivalent circuit impedance. For similar reasons, their amplitudes also have some differences. However, when angular displacements: α_l and α_r are considered individually, they will change randomly because they are influenced by the time range considered, the position of the fault on the rotor, the starting rotor position, and the rotor position evolution during the transient state to reach the speed mean value. Therefore, conventional bispectrum cannot represent this type of signal adequately, as discussed in Section 3.

Nevertheless, the amplitudes of the two sidebands will change with the degree of load/speed oscillation. When a reciprocating compressor operates under normal conditions the load fluctuation increases with the increase of discharge pressure. The change of the sidebands in both the amplitude and phase will change accordingly. This also means that if there is a fault in the compressor, the load fluctuation characteristics will be altered and hence the sidebands will be different from that when the compressor is healthy. Based on this analysis, the fault can be detected by a careful analysis of the current signal. Fig. 1 shows the current signals from a two-stage reciprocating compressor. The compressor has a 2.5 kW three-phase four-pole induction motor, a V-belt with a transmission ratio of 3.2 and a two-stage compressor operating in a pressure range from 80 to 120 psi (5.5 to 8.3 bar). From in-cylinder pressure waveforms and compressor torques, shown in Fig. 1(a) and (b), respectively, the motor is under a dynamic load fluctuating at about 7.3 Hz according to

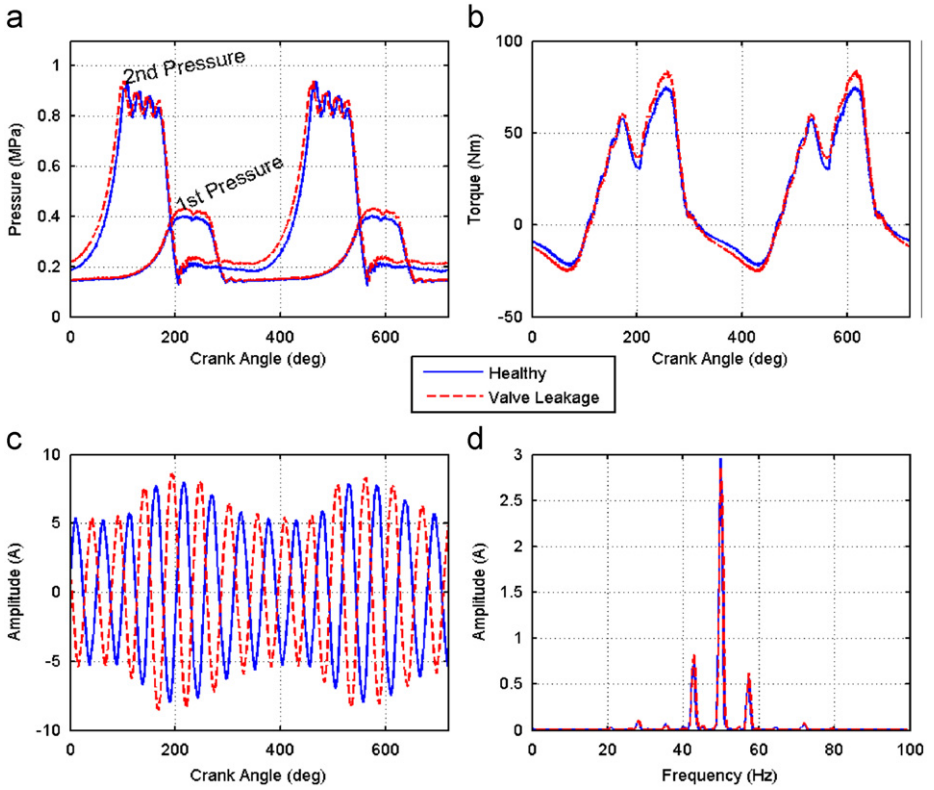

Fig. 1. Stator current waveforms and spectra for a healthy compressor and a valve leakage case: (a) cylinder pressures, (b) compressor torque, (c) stator currents and (d) current spectra.

the working cycle of the compressor. This fluctuating load leads to a modulated current waveform, shown in Fig. 1(c). The current waveforms exhibit certain amplitude modulation in line with the torque waveforms. The spectra of current signals, shown in Fig. 1(d), exhibit a high degree of AM feature. The carrier components at the supply frequency 50 Hz have very high amplitudes and the sideband components at 50 ± 7.3 Hz, which correspond to the working frequency of the compressor, are clearly visible.

More interestingly, the amplitude of the current waveform from the valve leakage seems slightly higher than that of a healthy condition. In the spectra, the sideband amplitudes for the leakage are also slightly higher whereas the supply amplitude has a small decrease when compared with the spectrum of the healthy condition. These are consistent with the changes in the pressure and torque graphs, which mean that the current signals contain sufficient information for compressor fault detection and diagnosis.

However, a compressor usually operates in a wide range of discharge pressures. The changes in current signals due to this operating condition often mask the small changes due to various incipient faults. This makes it difficult to classify and quantify different types of faults from normal conditions. This means that conventional second-order analysis, such as power spectrum and common waveform parameters, may be inefficient to discriminate the changes for motor current signal based fault diagnosis because only amplitude information from current signals are used by these methods. Therefore, more advanced signal processing methods have to be used to describe not only amplitude but also phase and nonlinear interaction in the current signal for enhancing the small changes for separating different types and severities of the compressor faults.

3. Performance of bispectrum

Bispectrum analysis has a number of unique properties such as nonlinear system identification; phase information retention and Gaussian noise elimination when compared with power spectrum analysis. Especially, bispectrum is used to detect quadratic phase coupling (QPC) which occurs when two waves interact non-linearly and generate a third wave with a frequency and phase equal to the sum (or difference) of the first two waves. As shown in Section 2, the current signal is formed by nonlinear combination from only two components: supply frequency and compressor working component. Thus it is anticipated that bispectrum can give a more accurate representation of the current signal for fault diagnosis. This section starts with examining the deficiency in applying the conventional bispectrum to current signals and modifies it based on the modulation feature of the current signal for more efficient representation.

3.1. Conventional bispectrum

Given a discrete time current signal $x(n)$, its discrete Fourier transform (DFT), $X(f)$ is defined to be

$$X(f)=\sum_{n=-\infty}^{\infty} x(n)e^{-j2\pi fn} \tag{11}$$

As it is a complex number, $X(f)$ can be rewritten in the format of magnitude $|X(f)|$ and ϕ_f:

$$X(f)=|X(f)|\,e^{j\phi_f} \tag{12}$$

From DFT, the conventional bispectrum $B(f_1, f_2)$ can be defined in the frequency domain as [16,19]

$$B(f_1,f_2)=E\left\langle X(f_1)X(f_2)X^*(f_1+f_2)\right\rangle \tag{13}$$

where $X^*(f)$ is the complex conjugate of $X(f)$ and $E\langle\,\rangle$ is the statistical expectation operator. f_1, f_2 and f_1+f_2 are three individual frequency components. Note that, unlike second-order measures, this third-order measure is a complex quantity in that it contains both magnitude and phase information about the original time signal $x(n)$. If the frequency components at f_1, f_2 and f_1+f_2 are independent components, each frequency will be characterized by statistically independent random phases distributed over $(-\pi, \pi)$. Upon statistical averaging denoted by the expectation operator $E\langle\,\rangle$ in Eq. (13), the bispectrum will tend towards zero due to the random phase mixing effect. In this way random noise can be suppressed significantly.

On the other hand, if the three spectral components: f_1, f_2 and f_1+f_2 are non-linearly coupled to each other, the total phase of the three components will not be random at all, even though each of the individual phases are random, in particular, the phases have the following relationship:

$$\phi(f_2)+\phi(f_1)=\phi(f_2+f_1) \tag{14}$$

Consequently, the statistical averaging will not lead to a zero value in the bispectrum. This nonlinear coupling is indicated by a peak in the bispectrum at the *bifrequency* $B(f_1, f_2)$.

To measure the degree of coupling between coupled components, a normalised form of the bispectrum or bicoherence is usually used and defined as [16]

$$b^2(f_1,f_2)=\frac{|B(f_1,f_2)|^2}{E\left\langle |X(f_1X(f_2))|^2\right\rangle E\left\langle |X(f_1+f_2)|^2\right\rangle} \tag{15}$$

The bicoherence is independent of the amplitude of the triple product of the DFT amplitudes and its values are bounded between 0 and 1. The bicoherence is close to 1 if there are nonlinear interactions among frequency combinations, f_1, f_2 and f_1+f_2. On the other hand, a value of near 0 implies an absence of interactions between the components. The possible amplitudes in the latter case may suggest that the components are originated independently from a system. Therefore, based on the amplitude of bicoherence the nonlinear interactions can be detected and the interaction degrees can be also measured between the coupling components.

Fig. 2 shows two bispectra and corresponding bicoherences of current signals for a healthy compressor and a valve leakage case, respectively. They are calculated through a direct method using fast Fourier transform (FFT). The spectral resolution is 0.5 Hz and the amplitude is averaged over 100 times. The two bispectra for both the healthy case and the valve leakage are very different. However, they all have a high peak at bifrequency (50, 50) and a number of small peaks which are separated by a frequency interval of 7.3 Hz, arising from the compressor working cycle and supply frequency. These features may thus indicate the nonlinear coupling effects existing in the current signals and make a difference between the normal and faulty case.

According to Eq. (13), the major component at (50, 50) results from the coupling between 50, 50 and 100 Hz. However, in theory the 100 Hz component should not exist in the signal if the compressor and driving motor are fault free and hence the component does not arise from nonlinear coupling. This can be confirmed by the coherences shown in Fig. 2(a2) and (b2). Their coherence amplitudes for both compressor cases are very low, which means that there is no nonlinear effect at bifrequency (50, 50) component. This also indicates that the presence of 100 Hz is due to background noise and spectral leakage from the finite length of DFT. Therefore, the bispectral peak at (50, 50) component is considered as a false peak or the conventional bispectrum is unable to reveal the nonlinear coupling effect in the current signal. This inefficiency of the conventional bispectrum has also been concerned in [24] by analysing a modulated signal from bearing vibration.

For similar reasons, the other bifrequency components with small peaks such as those at (50–7.3, 50) and (50, 50–7.3) cannot be taken as the nonlinear effects because their corresponding coherence amplitudes are too low. As discussed in Section 2, the phases of the sidebands and supply frequency vary with many influential factors and hence also changes between data frames in FFT calculation. The expectation average over different FFT frames will lead to a very small bispectrum magnitude at these bifrequencies. This shows that conventional bispectrum is not suitable for analysing the current signals from the compressor.

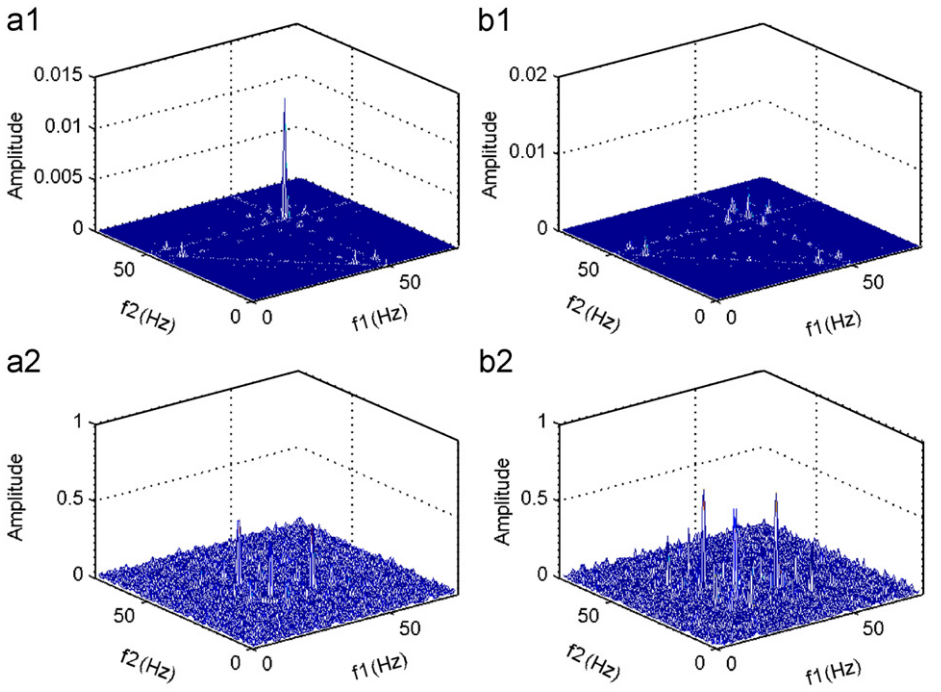

Fig. 2. Conventional bispectra for a healthy compressor and a valve leakage at 120 psi (8 bar): (a1) conventional bispectrum for healthy compressor, (a2) conventional coherence for healthy compressor, (b1) conventional bispectrum for valve leakage and (b2) conventional coherence for valve leakage.

3.2. Modulated signal bispectrum

From spectrum features of points, Eq. (13) includes only the presence of nonlinearity from the harmonically related frequency components: f_1, f_2 and f_1+f_2. It overlooks the possibility that the occurrence of f_1-f_2 may be also so due to the nonlinearity between f_1 and f_2. Because of this, it is not adequate to describe AM like signals such as motor current signals. To improve the performance of the conventional bispectrum in characterizing the motor current signals, a modified bispectrum, named an modulated signal bispectrum (MSB) is proposed in [14,15] as

$$B_{MS}(f_1,f_2)=E\left\langle X(f_2+f_1)X(f_2-f_1)X^*(f_2)X^*(f_2)\right\rangle \tag{16}$$

In the format of magnitude and phase, Eq. (7) can be rewritten as

$$B_{MS}(f_1,f_2)=E\left\langle |X(f_2+f_1)||X(f_2-f_1)||X^*(f_2)||X^*(f_2)|\,e^{j\phi_{MS}}\right\rangle \tag{17}$$

The total phase of MSB

$$\phi_{MS}(f_1,f_2)=\phi(f_2+f_1)+\phi(f_2-f_1)-\phi(f_2)-\phi(f_2) \tag{18}$$

As shown in Eq. (14), if two components f_1 and f_2 are in coupling, their phases are related as

$$\begin{aligned}\phi(f_2+f_1)&=\phi(f_2)+\phi(f_1)\\ \phi(f_2-f_1)&=\phi(f_2)-\phi(f_1)\end{aligned} \tag{19}$$

By substituting (19) into (18) the total phase of MSB will be zero and MSB amplitude will be the product of the four magnitudes, which is the maximum of the complex product. Therefore, a bispectral peak will appear at (f_1,f_2). Especially, Eq. (16) now takes into account both (f_1+f_2) and (f_1-f_2) simultaneously for measuring the nonlinearity in AM signals. If (f_1+f_2) and (f_1-f_2) are both due to nonlinear effect between f_1 and f_2, a bispectral peak will appear at bifrequency $B_{MS}(f_1,f_2)$. This is more accurate and efficient in representing the sideband characteristics of modulation signals. In addition, the four component products will enhance signal component more and produces more robust detection result to random noise.

Similar to the conventional bicoherence, a normalised form of MSB or modulated signal bicoherence is introduced as

$$b^2_{MS}(f_1,f_2)=\frac{|B_{MS}(f_1,f_2)|^2}{E\left\langle |X(f_2)X(f_2)X^*(f_2)X^*(f_2)|^2\right\rangle E\left\langle |X(f_2+f_1)X(f_2-f_1)|^2\right\rangle} \tag{20}$$

to measure the degree of coupling between three components in the same way as the conventional bicoherence.

3.3. Performance evaluation

To evaluate MSB performance, a numerical simulation is performed to compare its capability of characterizing AM signals with both the power spectrum and conventional bispectrum. To this end, a noise contaminated AM signal is generated as

$$x = A_L \cos(2\pi f_s t - f_L - \alpha_L) + A_c \cos(2\pi f_s t + \alpha_c) + A_U \cos(2\pi f_s t + f_U - \alpha_U) + A_n n(t) \quad (21)$$

where the carrier signal has an amplitude A_c=1, frequency f_c=50.01 Hz and a random phase α_c whereas the modulating signal has an amplitude A_L=A_U=0.01, frequency f_L=f_U=14.6 Hz and phases: α_L=$\alpha_c-\alpha_x$ and α_L=$\alpha_c+\alpha_x$ with random phases α_c and α_x from a uniform distribution between 0 and 2π. The noise $n(t)$ is from a normal distribution with 0 mean and standard deviation with a noise amplitude A_n=0.1. This signal is similar to measured current signals in which the carrier signal has much higher amplitude than that of sideband components and its frequency has a small deviation from nominal value of 50 Hz. For generating this signal, a sampling rate of 512 Hz was used. As shown in Fig. 3(a) this rate is sufficiently high to indicate the basic features of the AM signal exhibited in Fig. 1(c) but with more irregularity due to high noise contamination.

In analysing this signal, a data frame of 1024 was used in calculating both the power spectrum and the two types of bispectrum. In addition, a Hanning window is applied to the data frame to suppress spectral leakages due to the selection of the parameters in signal generation and calculations. In this way, this simulation will also help to determine the analysis parameters for measured signals.

Fig. 3(b) shows the power spectrum of the signal, which is obtained by averaging over 100 data frames. The AM feature may be identified by observing sideband peaks around the carrier components. However, because of the high level of background noise it may not be so definitive in recognizing the sidebands.

Fig. 4(a1) and (a2) show the results of the conventional bispectrum and its bicoherence, respectively. The bispectrum shows a distinctive peak at bifrequency (50.01, 50.01). However, its bicoherence does not have a corresponding peak to confirm the possible nonlinear interactions. Therefore, the peak is not from a true nonlinear interaction but from the interaction between the carrier component and the noise. Moreover, there is no sign to indicate the 14.6 Hz component seeded in the simulated signal, showing that it is impossible to detect the AM signal.

In contrast, the results of both the MSB and its bicoherence of the signal show a distinctive peak at bifrequency (14.6 and 50.01). Obviously, the MSB can reveal the nonlinear interaction between the carrier signal and the modulating signal and hence it is the most effective method of the three to characterize an AM signal with high noise contamination.

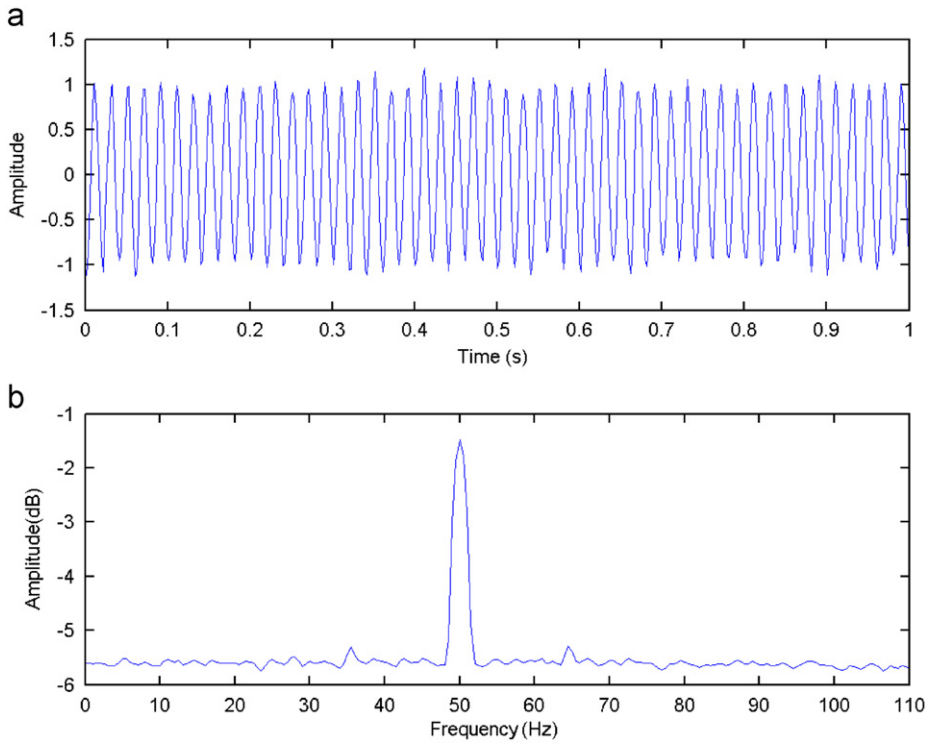

Fig. 3. A simulated AM signal and its power spetrum: (a) a segment of raw signal and (b) power spectrum.

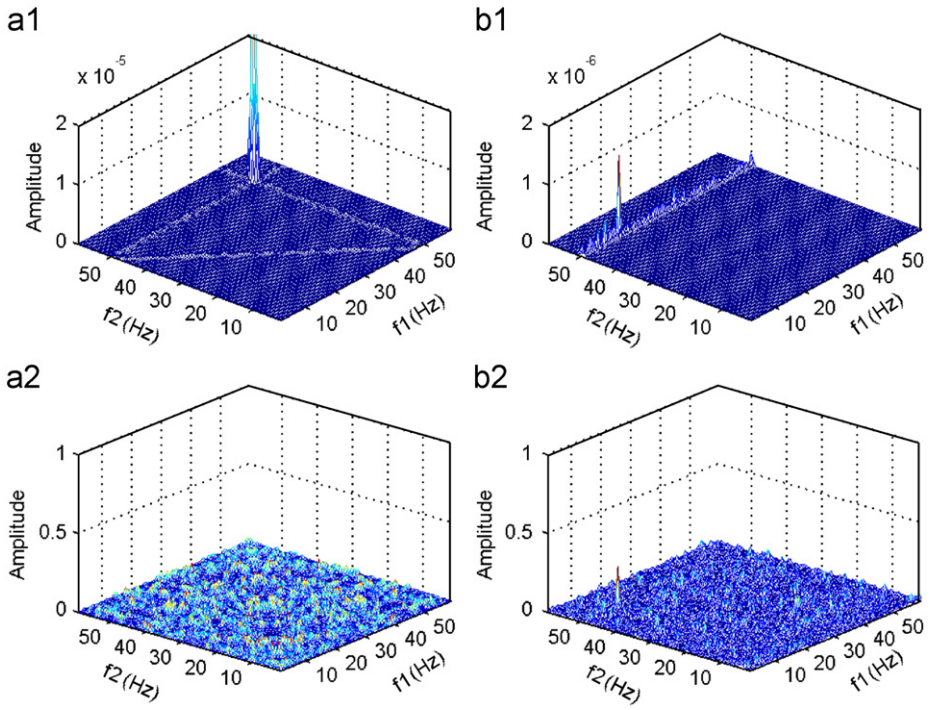

Fig. 4. MS bispectra of the simulated AM signal: (a1) conventional bispectrum, (a2) conventional bicoherence, (b1) MS bispectrum and (b2) MS bicoherence.

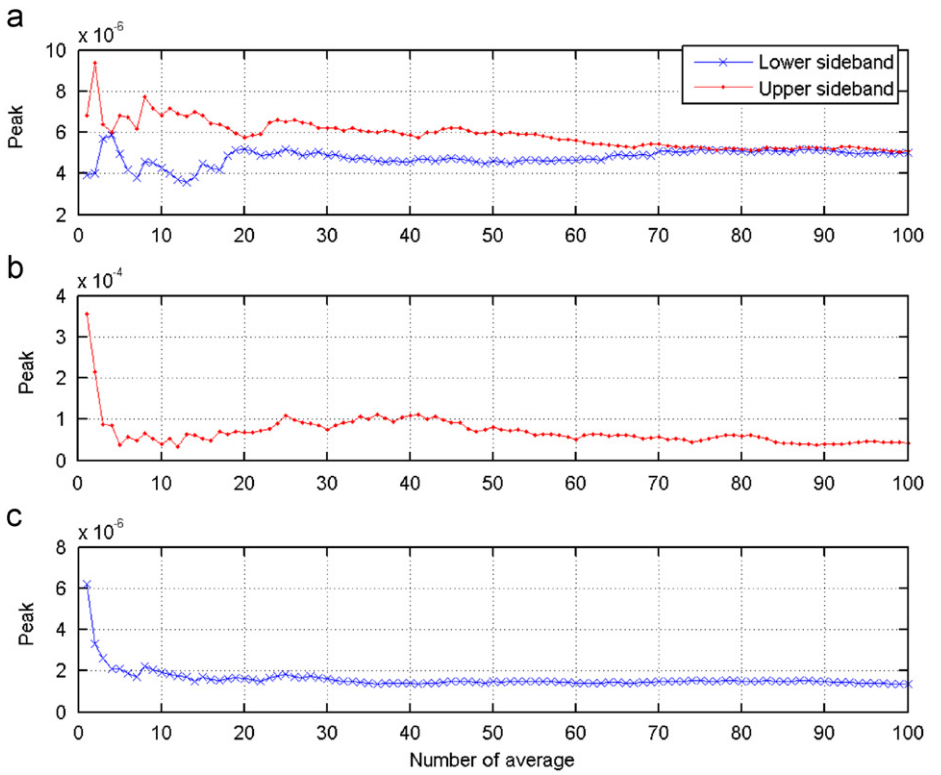

Fig. 5. Variation of peaks from power spectrum and bispectra with averages: (a) power spectrum, (b) conventional peak and (c) MS bispectrum.

In addition, the MSB also produces a more consistent estimation of the peak value. Fig. 5 shows the variation of peak values with the number of averages. The peak value from the MSB becomes very stable after the average number of 35 whereas the peak value from the conventional bispectrum continues to decrease as the average number increases. In the mean time the peaks of sidebands extracted from the power spectrum are also oscillating with the number of averages. In addition, an amplitude difference is significant between the lower and the upper sideband until 70 averages, which is not consistent with the simulated signal in that the sidebands are the same in amplitude.

This simulation shows that the MSB produces a much more reliable detection of the AM feature and produces more consistent and hence more accurate estimation of the peak values. Therefore, it outperforms the power spectral estimation in characterising the AM signal. In the mean time, it has also demonstrated that the conventional bispectrum may produce a misleading result and is not suitable for analysing AM signals.

4. Fault diagnosis

Based on the theoretical analysis and numerical study, it is confirmed that MSB is able to capture AM characteristics in signals more accurately. To examine its performance in characterizing measured signals for fault detection and diagnosis, it is thus applied to the motor current signals measured from the compressor with three common compressor fault cases: valve leakage, inter-cooler leakage and belt looseness, at different degrees and under different operating conditions.

4.1. Compressor fault cases

Discharge valve leakage, transmission belt looseness and inter-cooler leakage are three common faults in reciprocating compressors. The leakage is usually caused by thermal impacts and mechanical vibrations whereas the belt looseness is a typical feature when the texture of the belt has some damages. To evaluate the effectiveness of MSB in diagnosing these faults, these three faults are induced individually to the compressor with different degrees of severity. The valve leakage is introduced by drilling a 1 mm hole on valve plate for small leakage and a 2 mm hole for large leakage. The distance between two belt pulleys is reduced by 1 mm for small looseness and 2 mm for large looseness. However, only one case of inter-cooler leakage is induced because of the difficulty in adjusting the tightness of the connecting bolt for different degrees of leakage.

Fig. 6 shows the typical effects of the three types of fault on cylinder pressure and compressor torque for large degree cases. Because of compressed air backflow, the valve leakage shifts compression process earlier at the second stage and

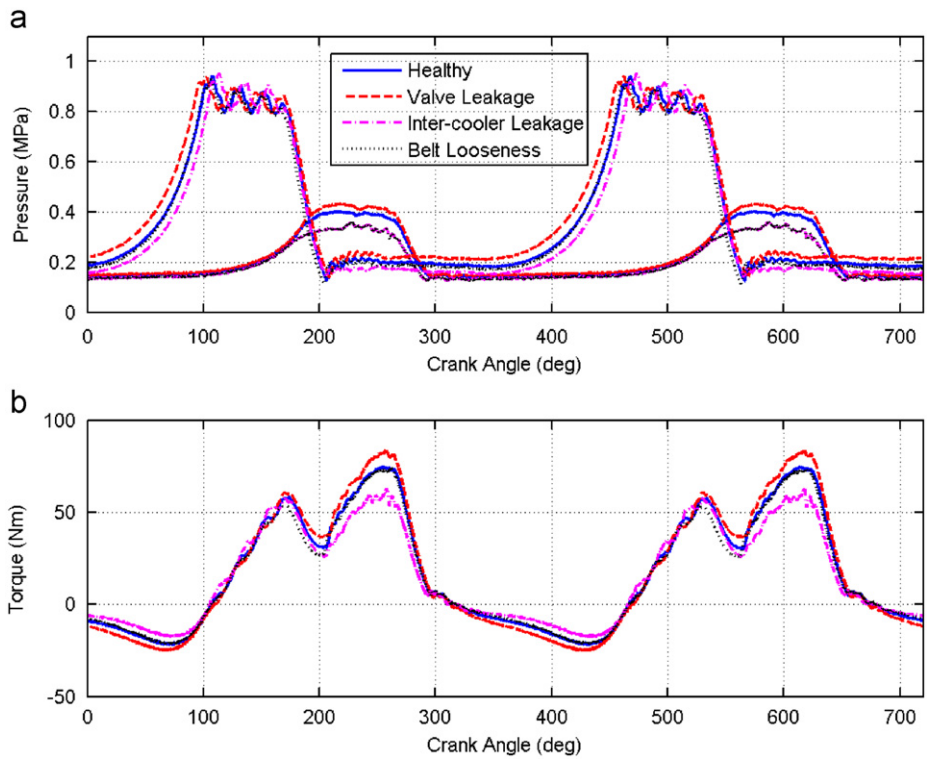

Fig. 6. Changes in cylinder pressure and compressor torque due to different faults: (a) cylinder pressure and (b) compressor torque.

cause a higher discharge pressure at the first stage. These pressure changes result in a higher dynamic torque and hence more nonlinear interactions in the current signal. On the other hand, the inter-cooler causes an inverse effect. It results in a smaller dynamic load and less nonlinear interactions. The belt looseness cases have no effect on the compressor pressure and load but it transfers a smaller dynamic load to the motor due to damping attenuation and slippage effects and hence results in much smaller nonlinear interactions in the current signal. This also means that any cylinder pressure change based detection methods such as pressure, vibration and temperature will be unsuccessful in detecting this type of fault. Moreover, these three seeded faults are very small. The compressor can produce the required pressure values without noticeable changes in its performance.

4.2. MSB analysis

Fig. 7 shows the MS bispectra and corresponding bicoherences for the healthy and the valve leakage, respectively, which are obtained from the same current signals as those discussed in Section 3.1. In the graphs, bispectrum peaks higher than 0.015 are truncated to 0.015 to illustrate smaller bispectrum peaks in the bispectrum graph. Even though the main peak at bifrequency (7, 3, 50) can be still found to be higher than the secondary peak at bifrequency (7.3, 50–7.3) as the wideness of the two peaks is clearly different. Comparing the healthy and faulty case, the amplitude of the main peak for faulty valve is about 30% higher than that of healthy case, showing that valve leakage produces higher nonlinear interaction between the compressor operating frequency and the fundamental component and hence indicating a more oscillating operation of the compressor.

In addition to the secondary peak bifrequency (7.3, 50–7.3), many other bispectrum peaks for both cases can be also observed undoubtedly. Bispectrum peaks at $(3 \times 7.3, 50)$ and $(2 \times 7.3, 50–7.3)$ are also clearly high. These peaks indicates that higher order harmonics of the compressor working frequency also cause nonlinear interactions and may be relied on for differentiating between faulty cases.

However, by checking the distribution of bicoherence, the coherence value at bifrequency (7.3, 50–7.3) is much smaller than 1. This indicates that this peak is influenced more by random noise than other peaks and thus it is not considered as a diagnostic feature. Moreover, the peaks at $(3 \times 7.3, 50)$ and $(50–7.3, 2 \times 7.3)$ for the faulty case are significantly higher than those of the healthy case, showing that nonlinear interactions also occur at higher frequencies and hence indicate the degree of load oscillation due to valve leakage.

According to Eq. (16), amplitudes of bispectrum slices at f_2=50 Hz will provide sufficient information to characterize the AM signal. So only the peaks at this slice will be examined for diagnosis feature development. In particular, only bispectrum peaks at $(n \times 7.3, 50)$ will be compared carefully between different fault cases. In addition, using one bispectrum slice for condition monitoring will reduce computational work significantly and hence the method can be implemented on-line with little improvement on the hardware resources used for power spectrum analysis.

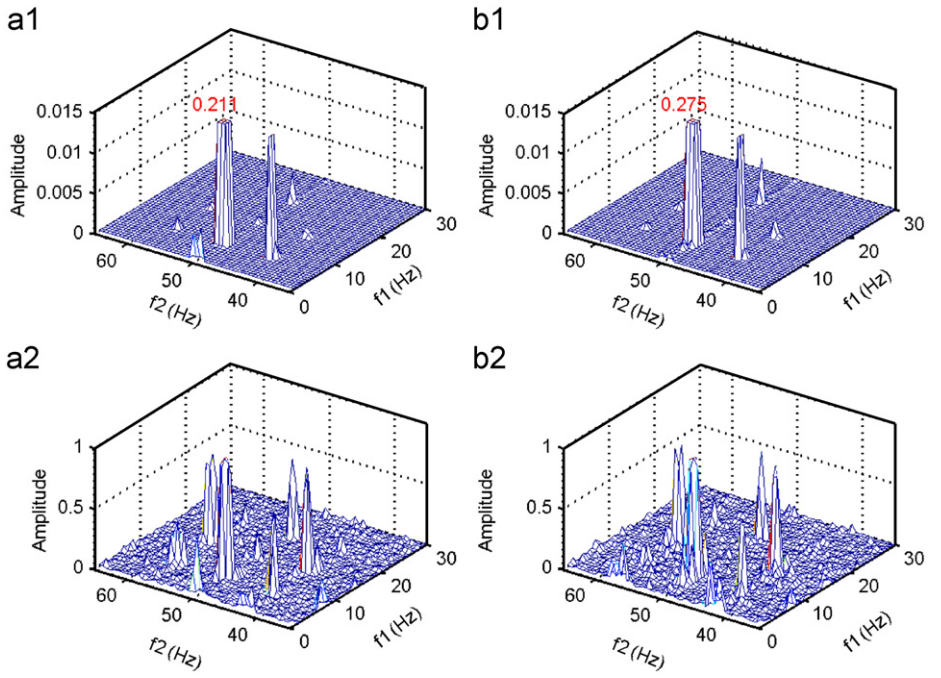

Fig. 7. MS bispectra for a healthy compressor and a valve leakage case at discharge pressure of 120 psi (8.2 bar): (a1) MS bispectrum for healthy compressor, (a2) MS coherence for healthy compressor, (b1) MS bispectrum for valve leakage and (b2) MS coherence for valve leakage.

Fig. 8 shows bispectrum slices of 50 Hz for all four compressor cases. Comparing the bispectrum peaks reveals that there are clear differences in the peak values between the healthy and faulty and between different faulty cases. In particular, valve leakage exhibits higher peak values whereas the other two types of faults: inter-cooler leakage and belt looseness, show lower values. Especially the belt loose case has significantly low peaks. These changes in bispectrum peaks are consistent with those in compressor torque waveforms illustrated in Fig. 6(b). The peak to peak value of the torque waveform is hither due to valve leakage whereas the peak value becomes lower due to the inter-cooler leakage. Therefore, both the main bispectrum peak and higher harmonic peaks can be used for discriminating different faults and fault severities.

4.3. Fault diagnosis

To diagnose the faults based on the MS bispectrum, two diagnostic feature parameters are developed based on the above analysis. The first one is obtained based on the bispectrum peak values. Rather using the peak values directly for separating different faults, an average value A_B around the peak is used to reduce the influence of spectral leakage, which is defined in the bispectrum domain as

$$A_B = \frac{1}{4k^2} \sum_{j=m-k}^{j=m+k} \sum_{i=n-k}^{i=n+k} A_{ij} \tag{22}$$

where (m, n) is the index of the peak position; k=4 is the number of the spectral lines around peak (m, n). To highlight further the effect of the 2nd order harmonics a 1.5 factor is applied to peak A_B^2 at the 2nd harmonics to combine it with the fundamental peak A_B^0. In addition, to reduce the dependency of the peak value on the discharge pressure the total peak amplitude is normalised by signal RMS value I_{rms}: to obtain a bispectral peak feature:

$$A_{Bn} = \frac{A_B^0 + 1.5A_B^2}{I_{rms}} \tag{23}$$

Obviously, a higher value of A_{Bn} shows a higher degree nonlinear interaction in current signals.

The second diagnostic feature is the signal kurtosis. Kurtosis is the zero-lag fourth cumulant normalised by the squared of signal variance. It also has the capability to highlight the high order statistics in the current signals. Investigations show that it performs better than other parameters such as RMS, skewness, and peak factors in discriminating the faults.

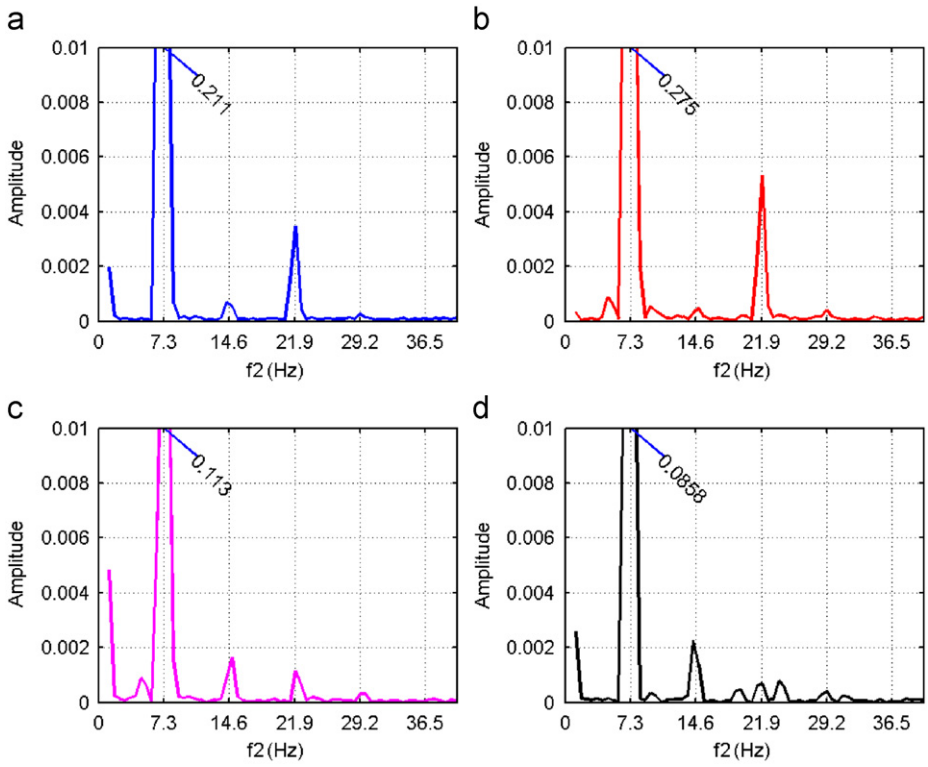

Fig. 8. MS bispectral slice of 50 Hz for healthy compressor and different faults at discharge pressure of 120 psi (8.2 bar): (a) healthy compressor, (b) valve leakage, (c) inter-cooler leakage and (d) belt looseness.

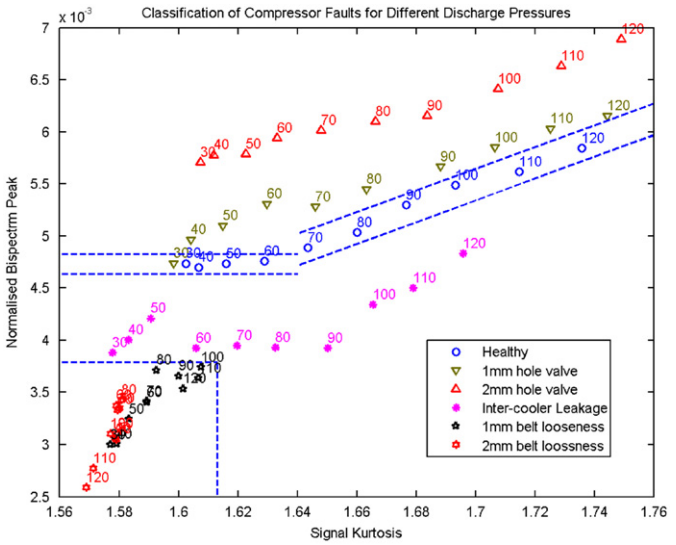

Fig. 9. Performance of compressor fault classification at different discharge pressure.

Therefore, kurtosis values are calculated and taken as a secondary feature in association with the normalised bispectral peak values for fault classification.

Fig. 9 shows the overall fault classification result under different discharge pressures using the two developed features. The classification can be carried out through two regions based on kurtosis amplitude. For kurtosis less than 1.64, which means weak nonlinear interaction, different types of faults can be separated by the amplitude of the bispectral peak features. A constant threshold can be set up to 4.8×10^{-3} and 5.5×10^{-3} for differentiating small and large valve leakage, respectively, whereas 4.6×10^{-3} and 3.8×10^{-3} can be used for separating inter-cooler leakage and belt looseness. However, different degrees of belt looseness cannot be separated completely even though the small belt looseness can be separated by higher bispectral peaks.

For kurtosis higher than 1.64, a linear classifier may be used for fault classification. The dashed lines with a positive slope in the graph show the intervals of 3 times of linear fitting residual. Any values exceeding this interval can be considered as faulty. The magnitude deviated from the region can be a measure of the fault severity. As shown in the figure, the large valve leakage has a larger deviation higher than the upper bound of interval, compared with the small leakage. For the inter-cooler leakage the deviation appears below the lower bound of the intervals.

Based on the above discussions, compressor fault diagnosis can be carried out at its rated operation range from 70 to 120 psi (4.8–8.2 bar) by a linear classifier whereas in a low pressure range from 30 to 70 psi (2–4.8 bar) by using a static threshold to check the value of the bispectral peak feature. In general, very low feature values can be used to differentiate the belt looseness from other fault cases. Different degrees of valve leakage and inter-cooler leakage can be separated easily using two constant thresholds as shown in the figure.

5. Conclusion

The analysis of the induction motor current signal with bispectrum clearly has significant potential as a means of non-intrusively detecting the presence of incipient faults in its driven equipment items by extracting the nonlinear interaction of linkage flux due to load variation. However, the conventional bispectrum is not adequate in representing the current signals with AM features because it cannot include sideband pairs simultaneously and the random variation of sideband phases. A modified bispectrum, i.e. MS bispectrum is then introduced to obtain a more accurate and efficient representation of the current signals. Based on the analysis, a normalised bispectral peak in conjunction with signal kurtosis is developed to diagnose common compressor faults including valve leakage, inter-cooler leakage and belt looseness. The classification results show that the low feature values can be used to differentiate the belt looseness from other fault cases and different degrees of valve leakage and inter-cooler leakage can be separated easily using two linear classifiers.

References

[1] W.T. Thomson, M. Fenger, Current signature analysis to detect induction motor faults, IEEE Industry Applications Magazine July/August (2001) 26–34.
[2] M.E.H. Benbouzid, A review of induction motors signature analysis as a medium for faults detection, IEEE Transactions on Industrial Electronics 47 (5) (2000) 984–993.

[3] R.R. Obaid, T.G. Habetler, R.M. Tallam, Detecting load unbalance and shaft misalignment using stator current in inverter-driven induction motors, in: IEEE International Electric Machines and Drives Conference, 2003, pp. 1454–1458.
[4] G.T. Honce, J.R. Thalimer, Reducing unscheduled plant maintenance delays—field test of a new method to predict electric motor failure, IEEE Transactions on Industry Applications 32 (3) (1996) 689–694.
[5] R.C. Kryter, H.D. Haynes, Condition monitoring of machinery using motor current signature analysis, Sound and Vibration (1989).
[6] K.N. Castleberry, S.F. Smith, A dedicated compressor monitoring system employing current signature analysis, ORNL Report DE 93010270.
[7] H. Fanglin, G. Songnian, Application of higher order cumulant to structure fault diagnosis, in: Proceedings of the 11th International Modal Analysis Conference, 1993, pp. 1237–1240.
[8] G. Gelle, M. Colas, G. Delaunay, Higher order statistics for detection and classification of faulty fan belts using acoustical analysis, in: IEEE Signal Processing Workshop on HOS, July 21–23, 1997.
[9] I.M. Howard, Higher-order spectral techniques for machine vibration condition monitoring, Proceedings of the Institution of Mechanical Engineers Part G 211 (1997) 211–219.
[10] N. Arthur, J. Penman, Induction machine condition monitoring with higher order spectra, IEEE Transactions on Industrial Electronics 47 (5) (2000) 1031–1041.
[11] M. Elhaj, F. Gu, A.D. Ball, A. Albarbar, M. Al-Qattan, A. Naid, Numerical simulation and experimental study of a two stage reciprocating compressor for condition monitoring, Mechanical Systems and Signal Processing 22 (2007) 374–389.
[12] R. Schoen, T. Habetler, Motor bearing damage detection using stator current monitoring, IEEE Transactions on Industry Applications 3 (1995) 6 (not in use).
[13] R.R. Schoen, G.T. Habetler, Effects of time varying loads on rotor fault detection in induction machines, IEEE Transactions on Industry Applications 31 (4) (1995).
[14] I.I. Jouny, R.L. Moses, Bispectra of modulated stationary signals, IEE Electronics Letters 30 (18) (1994) 1465–1466.
[15] J.R. Stack, R.G. Hartley, T.G. Habetler, An amplitude modulation detector for fault diagnosis in rolling element bearings, IEEE Transactions on Industrial Electronics 51 (5) (2004) 1097–1102.
[16] Y.C. Kim, E.J. Powers, Digital bispectral analysis and its applications to nonlinear wave interactions, IEEE Transactions on Plasma Science PS-7 (2) (1979) 120–131.
[17] F. Filippetti, G. Franceschini, C. Tassoni, AI techniques in induction machines diagnosis including the speed ripple effect, IEEE Transactions on Industry Applications 34 (1) (1998) 98–108.
[18] A. Bellini, F. Filippetti, G. Franceschini, C. Tassoni, G.B. Kliman, Quantitative evaluation of induction motor broken bars by means of electrical signature analysis, IEEE Transactions on Industry Applications 37 (5) (2001) 1248–1255.
[19] W.B. Collis, P.R. White, J.K. Hammond, Higher-order spectra: the bispectrum and trispectrum, Mechanical Systems and Signal Processing 12 (3) (1998) 375–394.
[20] C. Kar, A.R. Mohanty, Monitoring gear vibrations through motor current signature analysis and wavelet transform, Mechanical Systems and Signal Processing 20 (1) (2006) 158–187.
[21] J. Antonino-Daviu, P. Jover, M. Riera-Guasp, J. Roger-Folch, A. Arkkio, DWT analysis of numerical and experimental data for the diagnosis of dynamic eccentricities in induction motors, Mechanical Systems and Signal Processing, 21, , 2007 2575–2589.
[22] J. Antonino-Daviu, P. Jover Rodriguez, M. Riera-Guasp, M. Pineda-Sánchez, A. Arkkio, Detection of combined faults in induction machines with stator parallel branches through the DWT of the startup current, Mechanical Systems and Signal Processing, 23, , 2009 2336–2351.
[23] I. Tsoumas, A. Safacas, G..Vachtsevanos, Empirical mode decomposition of the stator start-up current for rotor fault diagnosis in asynchronous machines, in: Proceedings of the 2008 International Conference on Electrical Machines, 2008.
[24] F.E.H. Montero, O.C. Medina, The application of bispectrum on diagnosis of rolling element bearings: a theoretical approach, Mechanical Systems and Signal Processing 22 (3) (2008) 588–596.